Computer Engineering and Intelligent Systems
ISSN 2222-1719 (Paper) ISSN 2222-2863 (Online)
Vol 3, No.4, 2012

Quadrature Radon Transform for Smoother Tomographic Reconstruction

P. K. Parlewar (Corresponding author)
Ramdeobaba College of Engineering and Management
Gitti Khadan, Nagpur
Tel. : +91- 9665441651 E-mail : pallavi.parlewar10@gmail.com

K. M. Bhurchandi
Visvesvarya National Institute of Technology, Nagpur
Tel. : +91- 9822939421 E-mail : bhruchandikm@ece.vnit.ac.in

Abstract

Tomographic reconstruction using Radon projections taken at an angle $\theta[0,2\pi)$ introduce a redundancy of four. Hence the projection in one quadrant $\theta\ [0,\pi/2)$ are used for tomographic reconstruction to reduce computational overheads. In this paper, we present that the though the projections at an angle $\theta\ [0,\pi/2)$ do not introduce any redundancy, the achieved tomographic reconstruction is very poor. A qudrature Radon transform is further introduced as a combination of Radon transforms at projection angles θ and $(\theta+\pi/2)$. The individual back projections for θ and $(\theta+\pi/2)$ are computed in two parts separately; 1) considering them real and imaginary parts of a complex number 2) considering average of the individual back projections. It is observed that the quadrature Radon transform yields better results numerically and/or visually compared to conventional Radon transform $\theta[0,2\pi)$.

Keywords: Single quadrant Radon transform, quadrature Radon transform, Magnitude of complex projection, average, reconstruction.

1. Introduction

Tomography refers to the cross section imaging of an object from either transmission or reflection data collected by illuminating the object from many different directions one by one. In other words, tomographic imaging deals with reconstructing an image from its projections as presented by S. Chandra Kutter, *et. al* (2010). The exact reconstruction of a signal requires an infinite number of projections, since an infinite number of slices are required to include all of Fourier spaces. If however the signal have mathematical form then exact reconstruction is possible from limited set of projections as given by Meseresu and Oppenheim (1974). The first practical solution of image reconstruction was given by Bracewell (1956) in the field of radio astronomy. He applied tomography to map the region of emitted microwave radiation from the sun's disk. The most popular application is associated with medical imaging by use of computerized tomography (CT) in which the structure of a multidimensional object is reconstructed from set of its 2D or 3D projections (Grigoryan 2003). X-ray of human organs in which stack of several transverse projections are used to get the two dimension information which may be converted to three dimensions.

The selection of the projection set has attracted the researchers in various applications. Svalbe and Kingston (2003) presented selection of projection angles for discrete Radon transform from the known Farey fractions. It has been predicted in that all the Farey sequence points cannot be represented on Radon projections. This leads to a fact that the pixels in the annular and corner regions of an image tile are poorly represented in the projection domain with single set of projections. They also presented a generalized finite

Radon transform computation algorithm for NxN images using prime number size square tiles (Svalbe and Kingston (2007). The radon transform and its derivatives are useful for many image processing application such as denoising, locating linear features, detecting and isolating motion (Donoho 1997,Candes 1998, Candes and Donoho 1999) , Pattern recognition(Chen *et. al* (2005), image compression , and feature representation (Donoho and Vetterli 2003). Since all these applications of the Radon transform are in essence discrete, an accurate discrete formalism of the Radon transform is required. It will minimize the need for interpolating the projections and reconstructions. Though conceptualized in polar domain Finite Radon transform (FRT) is almost orthogonal (Donoho and Vetterli 2003). The FRT applies to square image data pxp where p is a small prime and assume the image is periodic with p in both the x and y direction, by defining the pxp array as the finite group Z_p^2 under addition. Both the Fourier slice theorem and convolution property hold for the FRT. Since p is prime there are only (p+1) distinct line directions (thus p+1 projections) corresponding to the p+1 unique subgroups. Every radial discrete line samples p points in the image and has p translates. It intersects any other distinct line only once. All these attributes match those of lines in continuous space as given by Kingston (2007).

In this paper, we consider the possibility of smoother reconstruction from a finite number of projections of the proposed quadrature Radon transform using two approaches. In the first approach, the two set of projections are taken from angle θ and (θ+$\boldsymbol{\pi}$/ 2) simultaneously and those two set of projections are considered as a real and imaginary part of a complex number. In another one, the individual back projections are averaged to yield smooth reconstruction. The proposed approaches yield better results compared to the single quadrant [0,$\boldsymbol{\pi}$ /2] Radon transform. Section 1 presents literature survey and organization of the paper. Section 2 explains forward Radon transform and its inverse i.e. back projection theorem with the help of Fourier slice theorem and Filter back projection. The anticipated Quadrature Radon Transform (QRT), its property and algorithm is given in section 3. Experiments and results are given in section 4. Finally conclusion is presented in section 5.

2. Radon Transform

Let (x, y) be coordinates of points in the plane. Consider an arbitrary integrable function *f* defined on domain *D* of real space $\mathbf{R^2}$. If *L* is any line in the plane, then set projections or finite line integrals of *f* along all possible lines *L* is defined as two dimensional Radon transform of *f* (Matus and Flusser 1993, Herman and Davidi 2008, Herman 1980) . Thus,

$$\check{f} = R_f = \int_L f(x,y)\, ds \qquad (1)$$

Where *ds* is an increment of length along *L*. The domain *D* may include the entire plane or some region of the plane as shown in Fig. 1. If *f* is continuous and has compact support then $\mathbf{R_f}$ is uniquely determined by integrating along all lines L. Obviously the discrete integral along line L, is the summation of the pixel intensities of D that fall on line L and is called a point projection. A set of point projections, for all lines parallel to L and with a fixed angle and spanning over D, is called a projection.

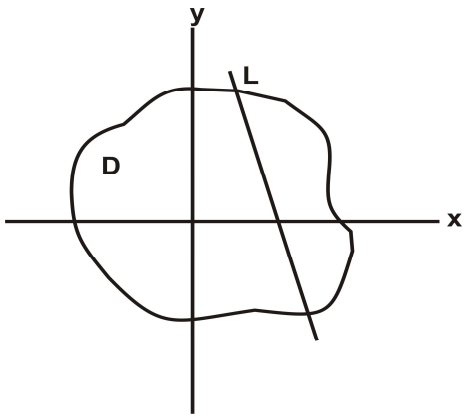

Fig. 1 Projection line L through domain D

In Fig.2 the projection line is considered perpendicular to a dotted line that passes through origin and intersects x axis at angle θ. The perpendicular distance between the line and the origin is p. A set of projections obtained due to integrals along all parallel projection lines perpendicular to the dotted line is called projection of D at an angle θ. Thus by changing the angle of the dotted line θ with x axis over the range [0 π/2), parallel projections for each value of θ can be obtained. This set of projections is called projections of D over the first quadrant. Similarly one can have projections of D over the remaining three quadrants.

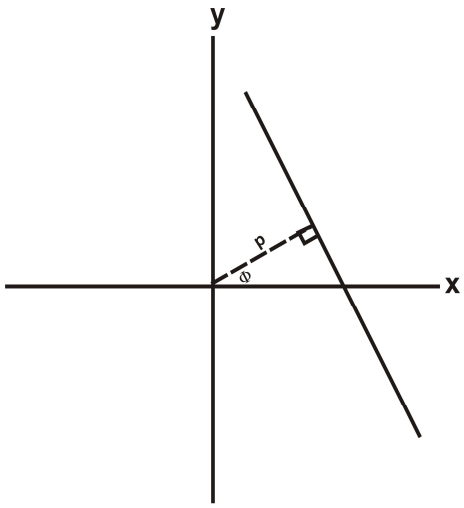

Fig. 2 Coordinates to describe the line in Fig. 1

The line integral depends on the values of p and Φ.

$$\check{f}(p,\phi) = R_f = \int_L f(x,y)\,ds \tag{2}$$

Thus, if $\check{f}(p,\phi)$ is finite for all p and Φ, then $\check{f}(p,\phi)$ is the two dimensional Radon transform of $f(x, y)$.

Now suppose a new coordinate system is introduced with axes rotated by an angle Φ, . If the new axes are labeled p and s as in Fig. 3, x and y can be re presented in terms of p and s using the shifting of reference mathematics as in (3).

$$x = p\cos\phi - s\sin\phi$$
$$y = p\sin\phi + s\cos\phi \qquad (3)$$

A somewhat clearer form of Radon transform can now be presented as in (4).

$$\check{f}(p,\varphi) = \int_{-\infty}^{\infty} f(p\cos\phi - s\sin\phi, p\sin\varphi + s\cos\phi)ds$$

()()w

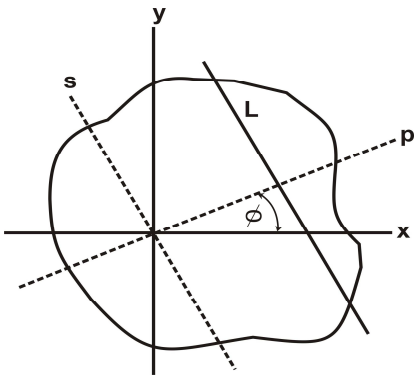

Fig. 3 The line in Fig. 2 relative to original and rotated coordinates.

Thus using (3) p may written as (5), if ξ is a unit vector in the direction of p.

$$p = \xi.x = x\cos\phi + y\sin\phi \qquad (5)$$

The parallel lines can be visualized as translated version of L using a translated dirac delta function $\delta(p-\xi x)$ along axis p as its multiplication with L. Then the transform may be written as an line integral over $\mathbf{R}^2$ by allowing the dirac delta function to select the line (5) from $\mathbf{R}^2$. Thus by modifying the above (4) we obtain (6)

$$\check{f}(p,\xi) = \int f(x)\delta(p-\xi\cdot x)\,dx \qquad (6)$$

Where ξ defines direction in terms of the angle ϕ. The (x, y) space for a fixed angle ϕ and the variable *p* changes along the direction defined by ξ.

2.1 Fourier slice theorem

Fourier slice theorem (FST) explains the reconstruction of the object from the projection data. Fourier slice theorem is derived by taking the one dimension Fourier transform of the parallel projections and noting that it is equal to the slices of the two dimensions Fourier transform of the object. The projection data should estimate the object using two dimensional inverse Fourier transform(Matus 1993, Portilla 2003, Hsung *et. al* 1996).

The simplest form of the Fourier slice theorem which is independent of the orientation between the object and the coordinate system is diagrammatically presented in Fig.4

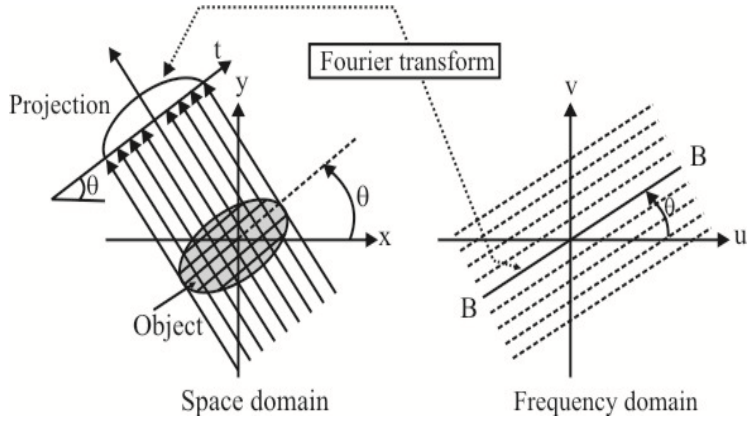

Fig. 4 Fourier Slice Theorem

In Fig (4) the (x,y) coordinate system is rotated by an angle *θ*. The FFT of the projection is equal to the 2-D FFT of the object slice along a line rotated by *θ*. Thus the FST states that, the Fourier transform of parallel projection of an image *f(x, y)* taken at an angle *θ* gives a slice of the 2-D transform, subtending an angle *θ* with the u-axis. In other words one dimensional FT of set of projections gives the value of two dimensional FT along lines BB in Fig. 4.

2.2. Filtered Back Projection

Filter back projection has two steps; the filtering part, which can be visualized as a simple weighting of each projection in the frequency domain, and the back projection part which is equivalent to finding the wedge shaped elemental reconstructions as presented by Hsung et. al (1996). Original image can be reconstructed exactly using the projections by applying filter and then taking the back projections (Kak and Slaney (2001). The process of filtered back projection can be explained as below

1) Apply a weighted filter, to the set of projections to obtained filtered projections.

2) Take back projections to obtain the exact reconstruction of the original image i.e. inverse radon transform algorithm

In the process of back projection, the filtered projection at a point t makes the same contribution to all pixels along the line L in the x-y plane. The resulting projections for different angles θ are added to form estimate of $f(x, y)$. To every point(x, y) in the image plane there corresponds a value t $(= x\cos\theta + y\sin\theta)$. This is shown from Fig. 5. It is easily seen that for the indicated angle θ, the value of t is the same for all (x,y) on the line L. Therefore, the filtered projection, Q_θ , will contribute equally to the reconstruction process. Thus each filtered projection Q_θ, is smeared back, or backprojected , over the image plane.

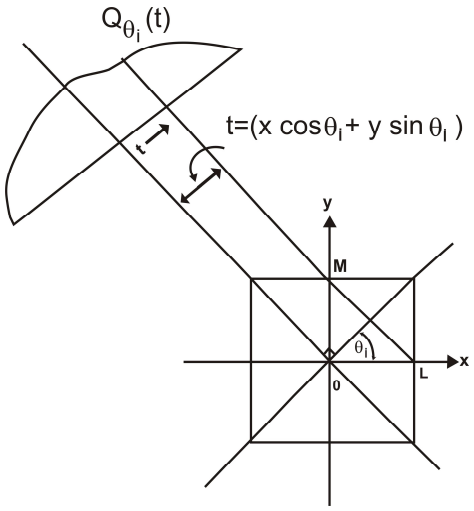

Fig.5 Reconstruction using back projection.

In Fig. 5a filtered projection is shown smeared back over the reconstruction plane along a line of constant t.

3. Quadrature Radon Transform

In most of the orthogonal image processing algorithms we consider image $f(x, y)$ as a separable function i.e. $f(x, y) = f(x) * f(y)$. Thus we first process the image along rows and then along columns i.e only in x and y direction and anticipate that the processing in x and y directions enough to approximate the processing all over the image in all possible directions. Obviously processing of a 2D variable will not fetch desired results with processing only in one direction. Radon transform of a 2D variable for angles $[0,\pi/2)$ is processing of the variable along line projections only in the first quadrant. Here we propose the Quadrature Radon transform, that takes projections on a line at an angle θ and also along a line perpendicular to it i.e. at $(\theta+\pi/2)$. Thus two sets of projections at right angles to each other are obtained. Let the continuous object f be approximated digitally within a four quadrant lattice and every quadrant is a digital array of lines, then the lines in the first quadrant and the third quadrant are parallel to each other. Similarly the projecton lines in the first and the third quadrant are parallel to each other. Obviously two sets of parallel projection lines on a discrete space is going to yield the same projection results. Thus two of the four quadrant projection sets may be the third and fourth quadrant are redundant and can be eliminated. Thus the projections in the first and the second quadrant have been considered for reconstruction using back projection algorithm. Eq. (7) and (8) present the sets of projections in the first and the second quadrant. The pixel array of an input

image results in two sets of projections; the first one for the first quadrant [0,π/2) and the second one for the second quadrant [π/2,π). Both the sets of projections are of equal size as that of the input pixel array. Thus, redundancy of only scale two is introduced as against four in case of Radon transform in four quadrants [0,2π).

$$\check{f}_1\left\{\check{f}:\theta_1 \in [0,\pi/2)\right\} = \int f_1(x)\,\delta(p-\xi\cdot x)\,dx \tag{7}$$

$$\check{f}_2\left\{\check{f}:\theta_2 \in [\pi/2,\pi)\right\} = \int f_2(x)\,\delta(p-\xi\cdot x)\,dx \tag{8}$$

In the first approach, the individual set of projections in each quadrant are considered real and imaginary parts of a complex entity. Thus (9) represents the proposed Complex Radon transform.

$$\check{f} = \check{f}_1 + j\ \check{f}_2 \tag{9}$$

If FBP represents filtered back projections of f, (10) and (11) represent the individual reconstructed versions of f using the filtered back projections.

$$f_1 = FBP(\check{f}_2) \tag{10}$$

$$f_2 = FBP(\check{f}_2) \tag{11}$$

Let f be the reconstructed signal using projections in both the quadrants. Using the first approach, it will be represented by (12). The reconstruction using the second approach is presented by (13).

$$f = \frac{1}{\sqrt{2}}\sqrt{f_1^2 + f_1^2} \tag{12}$$

In the second approach, the individual set of projections is considered independent. The first quadrant set of projections is considered in phase and the second quadrant set of projections is considered a quadrature component. Thus (7) and (8) jointly represent the proposed quadrature Radon transform.

While computing the inverse Radon transform, the back projection algorithm is applied on the two components resulting from (7) and (8) individually. (10) and (11) represent the sets of back projections i.e. the respective inverse Radon transforms.

$$f = \frac{f_1 + f_2}{2} \tag{13}$$

Theoretically, both should result in perfect reconstruction (Chen et. al. 2007) individually. But it is obvious that, a single set of projections in only one quadrant preserves the inter pixel relations only in one direction; either along rows or columns. Also, it poorly represents the corner pixels(Svalbe and Kingston 2003) . As a result the reconstruction using projections only in one quadrant is not accurate and smooth. The projections in more than one quadrant, rather at right angles to the first one will represent and preserve the inter pixel relations more accurately. The corner pixels' representation will also be improved as a result of averaging in spatial domain. Thus better tomographic reconstruction of the input image is obtained.

In the first approach, the resultant back projection is computed as magnitude of the complex number as presented in(12). In this approach, a normalization by a factor of ($2^{-1/2}$) is required to display the reconstructed image using 8 bit graphics. In the second approach, the resultant back projection is computed as average of the two individual back projections as presented in (13). In case of both the approaches the reconstructed images are better than the reconstruction from single quadrant projections.

4. Experiments

Initially, Radon transform of the gray and color test images have been computed using projections in the first quadrant i.e. from 0 to 89 degrees. Further, inverse Radon transform of the projection results has been taken using back projection theorem with different filters like 'bilinear', 'bicubic' etc to reconstruct original images. MSE and PSNR of the reconstruction have been computed. The reconstructed images are also observed visually. Further, radon transform of the same images were computed in the second quadrant using projections from 90 degrees to 179degrees. Original images are reconstructed using the projections in the second quadrant using different filtered back projections. MSE and PSNR of the reconstructed images using projections in the second quadrant are also computed. Using the first approach, the reconstructed image using the first quadrant and the second quadrant projections are then considered real and imaginary part of the reconstructed images respectively. The resultant magnitudes of the reconstructed images are computed using (12). MSE and PSNR of thus reconstructed images have been computed. In the second approach, average of the two reconstructed images using the first and second quadrant projections has been taken as final reconstructed image. MSE and PSNR of the reconstructed average image has been computed. These experiments have been repeated for several images but a few representative results and images reconstructed using the discussed and proposed algorithms have been presented in the next section.

5. Results

Results of the proposed forward and inverse Radon transform have been benchmarked with that of the Radon transform in the first quadrant i.e. [0, π /2). Table I presents MSE and PSNR of reconstructions with single quadrant and both quadrant projections on different color images using various filters before back projection.

Table 1 : Comparative performance of Single quadrant Radon reconstruction and the proposed Quadrature Radon Trans.

Image	Filter	Single Quadrant		Quadrature Radon (Complex)		Quadrature Radon (Average)	
		MSE	PSNR (db)	MSE	PSNR (db)	MSE	PSNR (db)
Peppers	Nearest	110.95	27.67	24.43	34.25	58.09	30.48
	Linear	110.96	27.67	23.36	34.44	54.19	30.79
	Spline	110.84	27.68	22.06	34.69	52.54	30.92
	Cubic	110.95	27.67	24.43	34.25	58.09	30.48
Pears	Nearest	114.75	27.53	38.46	32.28	75.29	29.36
	Linear	114.54	27.54	38.33	32.41	73.84	29.44
	Spline	114.30	27.55	38.68	32.60	71.54	29.58
	Cubic	114.36	27.54	38.40	32.51	72.53	29.52
Football	Nearest	112.46	27.62	23.36	34.44	57.13	30.56
	Linear	112.17	27.63	23.90	34.53	54.92	30.73
	Spline	112.04	27.64	23.87	34.73	53.80	30.82
	Cubic	112.09	27.63	23.30	34.64	54.31	30.78
Winters	Nearest	92.43	28.47	47.84	31.33	79.33	29.13
	Linear	92.99	28.49	47.24	31.38	77.33	29.24
	Spline	92.15	28.48	46.10	31.49	76.72	29.28
	Cubic	92.01	28.49	47.80	31.42	77.28	29.24
Baboon	Nearest	122.81	27.23	64.71	30.02	101.4	28.06
	Linear	122.16	27.26	62.49	30.17	98.02	28.21
	Spline	122.02	27.27	60.57	30.30	96.75	28.27
	Cubic	122.15	27.26	61.72	30.22	97.68	28.23

It is quiet obvious from Table I, that MSE for reconstruction using single quadrant is highest and accordingly PSNR is lowest as presented in column 3 and 4. In case of reconstructions using projections in the two quadrants and considering the individual back projected reconstructions as real and imaginary parts, the MSE is quiet low and PSNR is comparatively high as presented in column 5 and 6. Using average of the back projections in the two quadrants, the MSE and PSNR are moderate for all the reconstructed images. Thus numerically the reconstruction using single quadrant is poorest while using the first approach is the best.

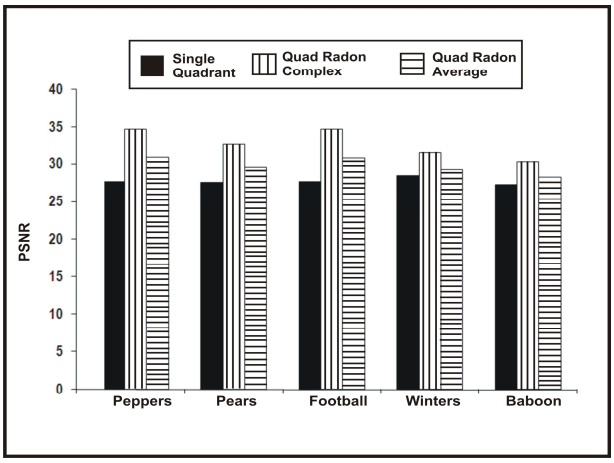

Fig, 6 Comparative Performance as in Table I, of the discussed techniques in bar chart form

Fig.7.(a)

Fig.7.(b)

Fig.7.(c)

Fig.7.(d)

Fig.7. (a) Peppers (b) Reconstructed using single Quadrant Radon projections (c) Reconstructed using Radon Complex number magnitude (d) Reconstructed using average of Quadrature Radon back projections

Fig.8.(a)

Fig.8.(b)

Fig.8.(c)

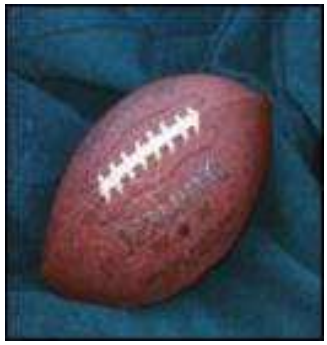

Fig.8.(d)

Fig.8. (a) Football (b) Reconstructed using single Quadrant Radon projections (c) Reconstructed using Radon Complex number magnitude (d) Reconstructed using average of Quadrature Radon back projections

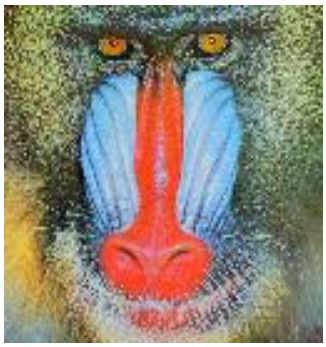

Fig.9.a

Fig.9.b

Fig.9.c

Fig.9.d

Fig.9.(a)Baboon (b)Reconstructed using single Quadrant Radon projections (c) Reconstructed using Radon-Complex magnitude (d) Reconstructed using average of Quadrature Radon back projections

Fig.10.(a)

Fig.10.(b)

Fig.10.(c)

Fig.10. (d)

Fig.6. (a) Peppers (b) Reconstructed using single Quadrant Radon projecttions (c) Reconstructed using Radon Complex number magnitude *(d)* Reconstructed using average of Quadrature Radon back projections

Fig. 6 presents the comparison of performance of the different techniques presented in Table 1 in the form of a bar chart. Fig. 7(a), Fig. 8(a), Fig. 9(a) and Fig 10.(a) present original color images Peppers, Football, Baboon and Winters. The images were transformed using single quadrant Radon projections and reconstructed using the same filtered back projections. Fig. 7(b), 8(b), 9(b) and 10 (b) present the results of reconstruction using the single quadrant projections. It is obvious that all these images are quiet distorted and hence unacceptable. Further projections were computed for the second quadrant. Reconstruction was done using (12) after taking back projections. The presented visual results in fig 7(c), 8(c), 9(c) and 10(c) indicate that the reconstructions using this approach are also unacceptable though numerically the MSE and PSNR are the best as presented in table 1. In the second approach, average of the two back projections was computed as in (13). It is observed that, though the MSE and PSNR are moderate, these results presented in Fig. 7(d), 8(d), 9(d) and 10(d) are the best visually.

6. Conclusion

Thus reconstruction using single quadrant Radon projections $[0,\pi/2)$ are not enough for accurate reconstruction. Both the proposed approaches yield numerically and visually better results compared to

reconstruction from only the projections in the first quadrant. The first approach of taking the magnitude of the two individual back projections considering them real and imaginary part of a complex number yields numerically better but visually poor results. However the second approach of taking average of the two individual back projections yields numerically moderate but visually the best results.

References

S. Chandra, N. Normand, N. Kingston, J. Guedon and I. Svalbe, (2010) " Fast Mojette transform for discrete tomography," *physics .med-ph, arXiv.org. arXiv*: 1006.1965v1 1. preprint 11.

R. M. Mersereau and A.V. Oppenheim, (1974) "Digital reconstruction of multidimensional signals from their projections," *in Proc. IEEE*, 62, 1319–1338.

A. M. Grigoryan,(2003) "Method of paired transform for reconstruction of images from projections: discrete model Image processing," *IEEE Trans. Image processing*, 12, 985-994.

R. N. Bracewell, (1956) "Strip integration in radioastronomy," Aust. J. Phys., 9, 198-217.

I. Svalbe and A. Kingston, (2003) "Farey sequences and discrete Radon transform projection angles," *Electronics Notes in Discrete Mathematics*, 12, 1-12.

A. Kingston and I. Svalbe, (2007) "Generalized finite radon transform for NxN images," *Image and vision computing*, 25, 1620-1630.

D. L. Donoho, (1997) "Fast ridgelet transforms in dimension 2," *in Stanford Univ. Dept. of Statistics, Stanford, CA, Tech. Rep.*

E. J. Candes, (1998) "Ridgelets : Theory and applications," *Ph.D.Thesis, Department of statistics, Stanford University.*

E. J. Candes and D. L. Donoho, (1999) "Ridgelets: a key to higher-dimensional intermittency?" *Phil. Trans. Roy. Soc. London*, 375, 2495-2509.

G. Y. Chen, T. D. Bui and A. Krzyzak, (2005) "Rotation invariant pattern recognition using Ridgelet, Wavelet cycle-spinning and Fourier features," *Pattern Recognition* 38, 2314-2322.

M. N. Do and M. Vetterli, (2003) "The finite Ridgelet transform for image representation," *IEEE Trans. Image Processing*, 12, 16-28.

F. Matus and J. Flusser, (1993) "Image representation via a finite Radon transform," *IEEE Trans. Pattern Analysis and Machine Intelligence*, 15, 996-1006.

G. T. Herman and R. Davidi , (2008) "Image reconstruction from a small number of projections," *IOP publishing, Inverse Problems*, 24, 1-17.

G. T. Herman, (1980) Image reconstruction from projections. *The fundamentals of computerized tomography. Newyork: Academic.*

J Portilla, (2003) "Image Denoising using Scale Mixture of Gaussians in Wavelet domain", *IEEE Trans. Image Process.*, 12, 11

T. Hsung, D. P. K. Lun and Wan-Chi Siu, (1996) "The discrete periodic Radon transform," *IEEE Trans. Signal processing*, 44, 2651-2657.

G. Y. Chen and B. Kegl, (2007) "Complex Ridgelets for Image Denoising" *Pattern Recg. ELSEVIER, Science direct*, 40, 578-585.

Kak and Slaney (2001), "Principals of computerized tomographic imaging," *Society of Industrial and Applied Mathematics*, pp. 1-86.